Quality Improvement of GaN on Si Substrate for Ultraviolet Photodetector Application

Chao-Wei Hsu, Yung-Feng Chen, and Yan-Kuin Su, *Fellow, IEEE*

***Abstract*— GaN is grown on an Si substrate using metal-organic vapor-phase epitaxy. Compared with the full width at half maximum values from X-ray diffraction patterns and photoluminescence spectra of conventional GaN on the Si substrate, those of GaN on the Si substrate with the insertion of various-temperature AlN nucleation layers and $Al_{0.3}Ga_{0.7}N$/GaN superlattice intermediate layers are reduced by 34.9% and 25.6%, respectively. In addition, Raman spectra show that residual stress on the GaN epilayers decreased by 0.35 GPa. The c-lattice parameter of the GaN epilayer is 5.1844 Å, which is close to that of an unstrained GaN layer. Ultraviolet metal-semiconductor-metal photodetectors are fabricated on an almost-crack-free GaN surface. The dark current of a photodetector on the Si substrate is 2.4×10^{-11} A at a 9 V applied bias, which is one order of magnitude smaller than that of a photodetector on a conventional sapphire substrate. The maximum quantum efficiency value of a photodetector on the Si substrate is ∼97% with an incident light wavelength of 360 nm and a 9 V applied bias.**

***Index Terms*— Metal–organic vapor–phase epitaxy, ultraviolet, photodetectors, GaN.**

I. Introduction

BOTH military and civilian applications require high–performance ultraviolet (UV) photodetectors (PDs). Gallium nitride (GaN), a semiconductor with a wide direct band gap (3.4 eV), high saturation velocity (2.7×10^7 cm/s), radiation hardness, and tolerability of aggressive environments, is well–suited for fabricating UV PDs [1], [2]. Various types of GaN–based PD have been proposed, such as p–n junction diode, p–i–n diode, Schottky diode, and metal–semiconductor–metal (MSM) PDs [3]–[7]. MSM PDs have an ultralow intrinsic capacitance, and their fabrication process is compatible with optoelectronic integrated circuits. Conventional GaN epilayers have been deposited on sapphire substrates, which are insulators with poor thermal conductivity and high cost [3]–[6]. Silicon (Si) substrates are more suitable for large–area applications due to their low cost. In addition, GaN–based MSM PDs prepared on an Si substrate can be integrated with field–effect transistor–based electronics on the substrate [1], [2]. However, the lattice constant mismatch and the difference in thermal expansion coefficient between Si and GaN often lead to poor crystal quality and the formation of crack networks [2], [8], [9]. In addition, it has been shown that Ga reacts strongly with Si, making it difficult to directly grow GaN on Si. To overcome these problems, a nucleation layer can be inserted between GaN and Si. Various nucleation layers, such as silicon carbide (SiC), aluminum nitride (AlN), aluminum arsenide (AlAs), and gallium arsenide (GaAs), have been used [7]–[11]. Among these nucleation layers, AlN is chosen in the present work because it can prevent Si from diffusing into the GaN epilayer and it effectively supports GaN hexagonal phase formation. However, the AlN nucleation layer creates a residual stress on the GaN surface due to the material mismatches between Si/AlN and AlN/GaN. The effects of the intermediate layer structure on the crystal quality of the GaN film and the performance of GaN PDs on an Si substrate have not been previously investigated.

In this paper, GaN is grown on Si substrates with various–temperature AlN (VT–AlN) nucleation layers and $Al_{0.3}Ga_{0.7}N$/GaN superlattice (SL) intermediate layers via metal–organic vapor–phase epitaxy. The materials grown are quantified and compared. UV GaN MSM PDs are fabricated on Si substrates and their optical and electrical properties are compared with those of GaN MSM PDs on sapphire substrates.

II. Experimental Details

200–mm, p–type, (111)–oriented Si substrates were used in this study. The samples were grown using an Aixtron metal–organic vapor–phase epitaxy system. TMGa, TMAl, TEGa, and NH_3 were used as precursors. For the AlN nucleation layer growth, the V/III ratio was about 1920, the chamber pressure was about in 101 mbar, the growth rate was around 2.5–2.7 nm/min. A 30–nm–thick AlN layer was initially grown on the Si substrate at 1393 K. Another 30–nm–thick AlN layer was then deposited at a temperature of 793 K to 1393 K. Subsequently, another 30–nm–thick AlN layer was deposited at 1393 K. $Al_{0.3}Ga_{0.7}N$/GaN SL layers were then grown at 1393 K with $Al_{0.3}Ga_{0.7}N$ and GaN thicknesses of 4 nm to 12 nm. $Al_xGa_{1-x}N$/GaN SL layers were then grown at 1393 K with $Al_xGa_{1-x}N$ compositions of $x = 0.1$ to $x = 0.5$. Finally, a 1–μm–thick GaN layer was deposited at 1393 K. The X–ray diffraction (XRD) ω scan rocking curves were obtained with a Bede D1 four–crystal diffractometer using Cu K_α radiation. The photoluminescence (PL) and Raman spectra were measured with a Jobin–Yvon LabRAM HR system using an He–Cd laser at 325 nm and an Argon laser at 514 nm as the excitation sources, respectively.

Manuscript received August 16, 2013; revised November 1, 2013; accepted November 16, 2013. Date of publication November 22, 2013; date of current version December 9, 2013. This work was supported in part by the Taiwan Semiconductor Manufacturing Company, Taiwan, in part by the National Science Council and Bureau of Energy, Ministry of Economic Affairs of Taiwan, under Contracts NSC 101-D0204-6 and NSC 100-2221-E-006-040-MY2, and in part by the LED Lighting Research Center of National Cheng Kung University, Taiwan.

The authors are with the Institute of Microelectronics, Department of Electrical Engineering and Advanced Optoelectronic Technology Center, National Cheng Kung University, Tainan 70101, Taiwan (e-mail: q1897124@mail.ncku.edu.tw; feng@cubic.mat.ncku.edu.tw; yksu@mail.ncku.edu.tw).

Digital Object Identifier 10.1109/JQE.2013.2292502

0018-9197 © 2013 IEEE

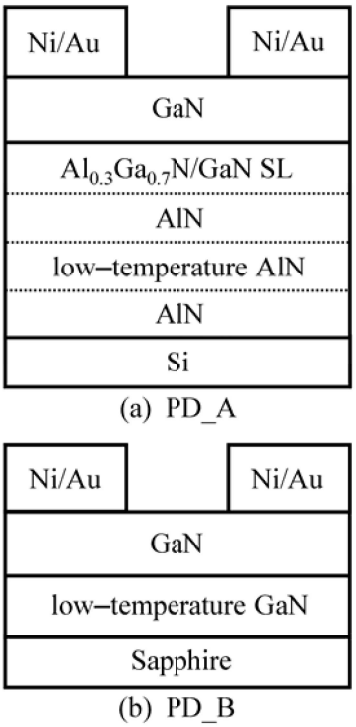

Fig. 1. Schematic diagrams of GaN-based MSM PDs with (a) GaN on Si substrate with VT-AlN nucleation layers and $Al_{0.3}GA_{0.7}N$/GaN SL intermediate layers and (b) GaN on sapphire substrate fabrication using the previously reported epitaxial processes.

The surface morphology was studied using field–emission scanning electron microscopy (SEM). A Pt–coated tip was used as a movable probe for atomic force microscopy (AFM), which was used to determine the surface roughness of the GaN surface. Ni(10 nm)/Au(90 nm) contact layers were then separately deposited on the samples using thermal evaporation and radio–frequency magnetron sputter systems. For comparison, previously reported epitaxial processes were used to deposit a 1–μm–thick GaN layer at 1393 K with a GaN nucleation layer at 813 K on a conventional sapphire substrate [3]–[6]. GaN MSM PDs were fabricated by using standard photolithography and lift–off processes. The electrode fingers of the interdigitated metal contact patterned on MSM PDs were 10 μm wide and 200 μm long, with a spacing of 10 μm. The samples were treated with rapid thermal annealing (RTA) at 1123 K for 90 s. A schematic of the structure is shown in Fig. 1. An HP–4156 semiconductor parameter analyzer was then used to measure the dark current–voltage (I–V) characteristics of these PDs. Spectral responsivity measurements were also conducted using a Jobin–Yvon SPEX system equipped with a 450–W xenon arc lamp light source and a standard synchronous detection scheme.

III. Results and Discussion

The VT–AlN nucleation layer structure contains two high–temperature AlN layers and one low–temperature AlN layers, as shown in Fig. 1(a). Regarding epitaxial parameters, a lower growth rate decreases the probability of stacking faults, interstitial impurities, and substitutional impurities, resulting in better crystal quality [2], [8], [12]. During the epitaxial processes, a high V/III ratio contributes to enhance epitaxial lateral growth resulting in dislocation bending and good epilayer uniformity [2], [13], [14]. A lower chamber pressure leads to a smaller amount of impurity, pollution, and carrier gas consumption [8], [12], [14]. A low chamber pressure, a low growth rate, and a high V/III ratio were thus used here. The growth temperature of the nucleation layer affects the organic precursor molecular pyrolysis, chemical reactant diffusion, atom bond strength to the substrate surface, and crystal coalescence [12], [14]. A large thermal expansion coefficient mismatch between materials and high thermal stress during the epitaxial procedure create lots of cracks [2], [8], [15]. In this work, the low–temperature AlN nucleation layer was deposited at various temperatures, and the resulting crystal qualities were compared. Table I lists the full width at half maximum (FWHM) values of XRD rocking curves of the (002) reflection, FWHM values of PL measurements, and GaN roughness values. Lower FWHM values of XRD patterns and PL spectra mean lower defects and impurities in the epilayer, and thus better crystal quality [8], [12]. A smoother surface also means lower density of defect pits and cracks.

TABLE I
Specifications of GaN on Si Substrate With Low-Temperature AlN (LT-AlN) Nucleation Layers Deposited at Various Temperatures

Sample	Temperature of LT–AlN (K)	FWHM of XRD (arcsec)	FWHM of PL (eV)	Roughness (nm)
S0	1393 K	757	0.043	7.7
S1	1193 K	720	0.041	6.9
S2	1093 K	601	0.038	6.1
S3	993 K	564	0.034	4.2
S4	893 K	588	0.037	5.7
S5	793 K	652	0.041	7.5

For the low–temperature AlN nucleation layer deposited at 1393, 1193, 1093, 993, 893, and 793 K (samples S0, S1, S2, S3, S4, and S5, respectively), the FWHM values of the XRD rocking curves are 757, 720, 601, 564, 588, and 652 arcsec, respectively. This crystal quality trend is similar to those of surface roughness and FWHM values of PL spectra. Depositing the low–temperature AlN nucleation layers at 993 K yielded the best crystal quality. Compared with the FWHM values from XRD patterns and PL spectra of conventional GaN on an Si substrate using high–temperature AlN nucleation layers (sample S0), those of GaN on an Si substrate using low–temperature AlN nucleation layers (sample S3) are significantly reduced by 25.5% and 20.9%, respectively. In addition, the surface roughness of the GaN epilayers is reduced by 45.5%. The VT–AlN nucleation layer effectively lowers the influence of the thermal expansion coefficient mismatch, resulting in crystal quality improvement. Dadgar *et al.* reported a FWHM value of the XRD for a GaN grown on Si of about 986 arcsec [16]. Liang *et al.* reported a FWHM value of the XRD for a 1.5 μm thick GaN on Si with a H.T. AlN nucleation layer and a long time thermal annealing step

TABLE II
SPECIFICATIONS OF GaN ON Si SUBSTRATE WITH $Al_{0.3}Ga_{0.7}N$/GaN SL INTERMEDIATE LAYERS WITH VARIOUS THICKNESSES AND PERIODS

Sample	Thickness and number of pairs of $Al_{0.3}Ga_{0.7}N$ / GaN (nm)	FWHM of XRD (arcsec)	FWHM of PL (eV)	Roughness (nm)
S6	(8 nm/ 0 nm) ×20 pairs	548	0.034	4.0
S7	(8 nm/ 4 nm) ×20 pairs	493	0.032	3.2
S8	(8 nm/ 8 nm) ×20 pairs	513	0.032	3.6
S9	(8 nm/12 nm)×20 pairs	524	0.034	3.8
S10	(0 nm/ 4 nm) ×20 pairs	562	0.034	4.2
S11	(4 nm/ 4 nm) ×20 pairs	520	0.032	3.7
S12	(12 nm/4 nm)×20 pairs	539	0.034	4.4
S13	(2 nm/ 1 nm) ×20 pairs	575	0.038	5.9
S14	(4 nm/ 2 nm) ×20 pairs	539	0.033	4.3
S15	(12 nm/8 nm)×20 pairs	515	0.032	3.9
S16	(8 nm/ 4 nm) ×10 pairs	523	0.033	3.8
S17	(8 nm/ 4 nm) ×30 pairs	507	0.032	3.6
S18	(8 nm/ 4 nm) ×40 pairs	531	0.034	4.6

TABLE III
SPECIFICATIONS OF GaN ON Si SUBSTRATE WITH $Al_xGa_{1-x}N$/GaN Sl INTERMEDIATE LAYERS WITH VARIOUS $Al_xGa_{1-x}N$ COMPOSITIONS

Sample	Composition of $Al_xGa_{1-x}N$ / GaN (8 nm / 4 nm)×20 pairs	FWHM of XRD (arcsec)	FWHM of PL (eV)	Roughness (nm)
S7	x = 0.3	493	0.032	3.2
S19	x = 0.1	551	0.035	4.1
S20	x = 0.2	512	0.032	3.8
S21	x = 0.4	532	0.034	4.0
S22	x = 0.5	579	0.038	6.0

(for 20 min at 923 K) of about 583 arcsec, which is higher than that obtained from here (sample S3) [17].

$Al_{0.3}Ga_{0.7}N$/GaN SL layers with various thicknesses were then deposited, and the improvements in the crystal quality of GaN were compared. Table II lists some FWHM values of XRD rocking curves of the (002) reflection, FWHM values of PL measurements, and GaN roughness values. The FWHM values of XRD rocking curves for samples S6, S7, S8, S9, S10, S11, and S12 are 548, 493, 513, 524, 562, 520, and 539 arcsec, respectively. This crystal quality trend is similar to those of surface roughness and the FWHM values of PL spectra. The best crystal quality was obtained for the $Al_{0.3}Ga_{0.7}N$/GaN SL layers with $Al_{0.3}Ga_{0.7}N$ and GaN thicknesses of 8 and 4 nm, respectively. $Al_{0.3}Ga_{0.7}N$/GaN SL layers with various single–pair thicknesses of 3, 6, 12, and 20 nm (samples S13, S14, S7, and S15, respectively) were then compared. $Al_{0.3}Ga_{0.7}N$/GaN SL layers with periods of 10, 20, 30, and 40 pairs (samples S16, S7, S17, and S18, respectively) were also compared. The sample S13 shows bed crystal quality. It's suggested that the induced force by the strain–layer SL structures are not suitable to repulse the dislocations away [12], [15], [20]. For $Al_xGa_{1-x}N$/GaN SL layers with an x ratio of 0.1, 0.2, 0.3, 0.4, and 0.5 (samples S19, S20, S7, S21, and S22, respectively), the FWHM values of the XRD rocking curves are 551, 512, 493, 532, and 579 arcsec, respectively. The resulting crystal qualities are listed in Table III. An Al content of 30% and a Ga content of 70% are well matched for the $Al_{0.3}Ga_{0.7}N$/GaN SL structure. This SL composition may provide good atom arrangements during lattice formation and give suitable compensative strain to decrease the residual strain of the epilayer resulting in good crystal quality [2], [8], [12], [15]. The insertion of $Al_xGa_{1-x}N$/GaN SL layers create a strain to decrease the residual stress of the epilayer [15]. A suitable $Al_xGa_{1-x}N$/GaN SL structure, with the proper layer thicknesses, composition, and number of pairs, can effectively decrease treading dislocations and stacking faults of lattice atoms, resulting in crystal quality improvement [15], [18], [19]. For the hetero–epitaxial growth, the stresses and strains are among the biggest challenges due to lattice constant mismatch and thermal expansion constant mismatch [15]. Theoretical models suggest the possibility of dislocation reduction and strain relief with the insertion of a suitable SL interlayer [2], [8], [12], [15], [20], [21]. However, in practice, suitable AlGaN/GaN SL structures must be tuned for better GaN crystal quality. In this work, the best crystal quality was obtained with 20 pairs of $Al_{0.3}Ga_{0.7}N$/GaN SL layers and $Al_{0.3}Ga_{0.7}N$ and GaN thicknesses of 8 and 4 nm, respectively. The corresponding surface roughness, and XRD and PL FWHM values are 3.2 nm, 493 arcsec, and 0.032 eV, respectively. Compared with the FWHM values from XRD patterns and PL spectra of conventional GaN on an Si substrate, those of GaN on an Si substrate with the insertion of VT–AlN nucleation layers and $Al_{0.3}Ga_{0.7}N$/GaN SL intermediate layers are reduced by 34.9% and 25.6%, respectively. In addition, the surface roughness of the GaN epilayers is significantly reduced. Yu *et al.* reported a FWHM value of the PL peak for a 1–2 μm thick GaN on Si with a H.T. AlN nucleation layer of about 0.0447 eV [22]. Huang *et al.* reported an FWHM value of the XRD peak for GaN on Si with a step–graded AlGaN intermediate layer of about 690 arcsec, which is higher than that obtained here [11].

Fig. 2(a)–(c) show SEM images of the GaN surface of samples S0, S3, and S7, i.e., GaN on Si without VT–AlN and without $Al_{0.3}Ga_{0.7}N$/GaN SL layers, with VT–AlN and without $Al_{0.3}Ga_{0.7}N$/GaN SL layers, and with VT–AlN and $Al_{0.3}Ga_{0.7}N$/GaN SL layers, respectively. The sample S0 has a lot of cracks on the GaN surface, indicating poor crystal quality. Some of these cracks were caused by the residual stress created by the mismatch of the thermal expansion coefficient between GaN and Si. The cracks for GaN on Si with VT–AlN are much fewer than those for GaN on Si with only the high–temperature AlN intermediate layer. When both VT–AlN and $Al_{0.3}Ga_{0.7}N$/GaN SL intermediate layers were used in the growth of GaN/Si, the GaN surface was almost crack–free. Fig. 3 shows Raman spectra of the three samples measured at room temperature. In these three spectra, the peaks near 564.9, 565.9, and 566.4 cm^{-1} of samples S0, S3, and S7, respectively, originate from the E_2 mode of the GaN hexagonal phase. It has been shown previously that the E_2 mode Raman peak of unstrained hexagonal GaN is located at 567.4 cm^{-1} [23]. In other words, the Raman peak

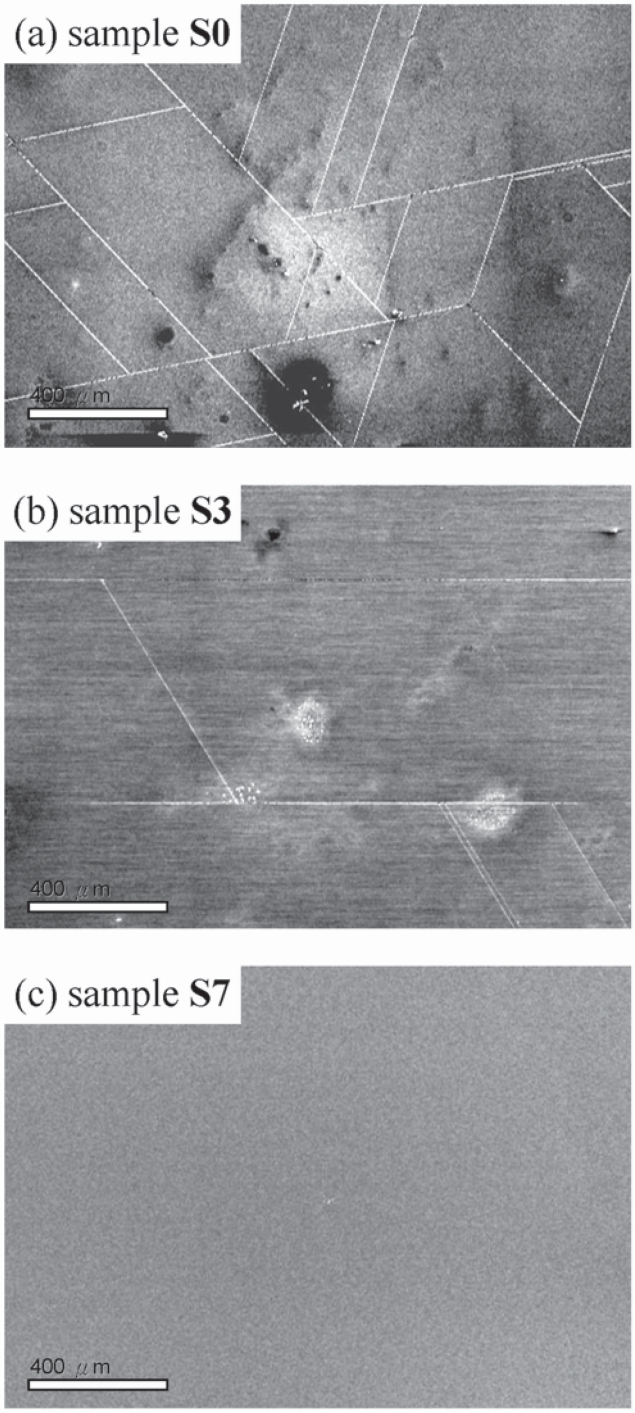

Fig. 2. SEM surface images of GaN on an Si substrate (a) without VT-AlN and without $Al_{0.3}GA_{0.7}N$/GaN SL layers, (b) with VT-AlN and without $Al_{0.3}GA_{0.7}N$/GaN SL layers, and (c) with VT-AlN and $Al_{0.3}GA_{0.7}N$/GaN SL layers.

position is red–shifted by 2.5, 1.5, and 1.0 cm^{-1} for samples S0, S3, and S7, respectively. The relationship between the E_2 mode Raman peak shift ($\Delta\omega_\gamma$) and the in–plane biaxial stress ($\sigma_{\chi\chi}$) can be expressed as [7], [23], [24]:

$$\sigma_{\chi\chi} = \Delta\omega_\gamma / K_\gamma \tag{1}$$

where $\sigma_{\chi\chi}$ is the stress in GPa, $\Delta\omega_\gamma$ is the Raman peak shift in cm^{-1}, and K_γ is the stress coefficient (4.3 cm^{-1} GPa^{-1}).

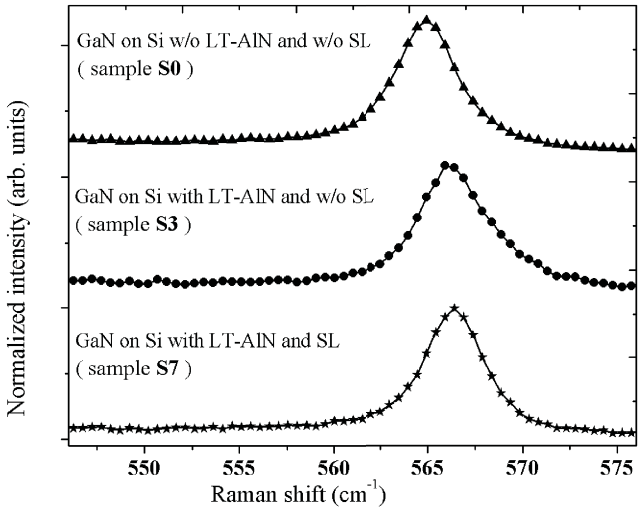

Fig. 3. Raman spectra of three samples measured at room temperature.

The stress values on the GaN surface are estimated as 0.58, 0.35, and 0.23 GPa for samples S0, S3, and S7, respectively. These results indicate that the residual stress is reduced by about 0.35 GPa on the GaN surface for GaN deposited on an Si substrate with VT–AlN and $Al_{0.3}Ga_{0.7}N$/GaN SL intermediate layers. The c–lattice parameter of the GaN layer can be measured using XRD [25]. The c–lattice parameter values, $\overline{C}_r$, are determined as 5.1763, 5.1821, and 5.1844 Å for samples S0, S3, and S7, respectively. The out–of–plane strain component, ε_c, of the GaN layer can be expressed as [25], [26]:

$$\varepsilon_c = \frac{\overline{C}_r - C_0}{C_0} \tag{2}$$

where C_0 is c–lattice parameter of the unstrained GaN layer (5.1850 Å) [25]. The strain components for samples S0, S3, and S7 are evaluated as -1.68×10^{-3}, -5.59×10^{-4}, and -1.16×10^{-4}, respectively. These results indicate that the strain is reduced in the GaN layer for GaN deposited on an Si substrate with VT–AlN nucleation layers and $Al_{0.3}Ga_{0.7}N$/GaN SL intermediate layers. The trend of strain reduction shown in the XRD results corresponds with the stress reduction shown in the Raman results. These results indicate an almost–crack–free GaN surface.

GaN MSM PDs were fabricated on Si substrates with VT–AlN and $Al_{0.3}Ga_{0.7}N$/GaN SL layers (i.e., PD_A in Fig. 1(a)). For comparison, GaN MSM PDs on a sapphire substrate were also prepared (i.e., PD_B in Fig. 1(b)). The epilayer of sample PD_B has XRD FWHM, PL FWHM, and surface roughness values of about 509 arcsec, 0.033 eV, and 3.7 nm, respectively. A high–work–function Ni/Au electrode was used to ensure a high Schottky barrier high. The RTA steps are used to enhance the metal–semiconductor contact. Fig. 4(a) shows the I–V characteristics of PD_A and PD_B measured in the dark. With a 5–V applied bias, the measured dark current (leakage current) of PD_A is 1.5×10^{-11} A. The dark current of PD_A is 2.4×10^{-11} A under a 9–V applied bias. With 5–V and 9–V applied biases, the measured dark currents of PD_B are 2.5×10^{-10} and 5.6×10^{-10} A, respectively.

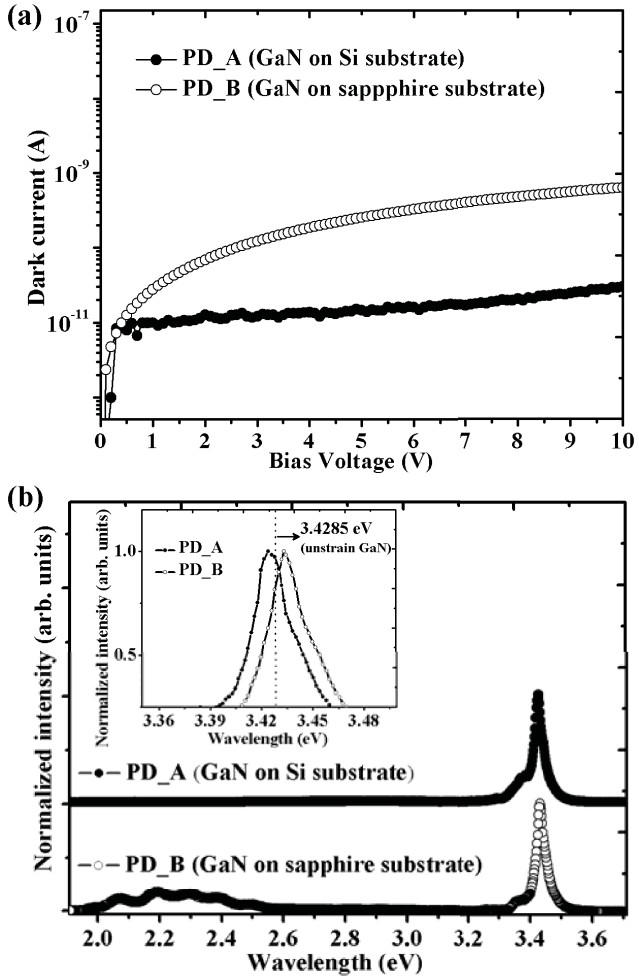

Fig. 4. (a) *I-V* characteristics of PD_A and PD_B measured in the dark. (b) PL spectra of PD_A and PD_B. The inserted figure shows the intense near-band-gap transition region.

Chiang *et al*. reported a dark current of above 10^{-7} A at a 9–V applied bias for GaN MSM PDs on Si substrates with a β–SiC intermediate layer [7]. Chang *et al*. reported a dark current of above 3.0×10^{-10} A at a 5–V applied bias for GaN MSM PDs on a sapphire substrate [3], [4]. These values are higher than that of PD_A. A large leakage current can be attributed to the trapping of minority carriers at the metal–semiconductor interface [27]. The trapped carriers reduce the depletion width and the build–in voltage, lowering the Schottky barrier height and thus increasing the leakage current [6]. This implies that PD_A has a lower number of trapped states at the GaN surface than that of PD_B. Fig. 4(b) shows the PL spectra of the two samples. An intense near–band–gap transition is located at 3.4 eV. Fig. 4(b) shows a second luminescence line centered at around 2.2 eV for PD_B, which represents yellow luminescence due to a transition from shallow to deep donor states. The optical absorption related to the yellow band is attributed to a transition from impurity levels, called defect trapped levels or trapped states, to the conduction band [28], [29]. There are thus fewer trapped states on the GaN surface of PD_A than on PD_B. Sheu *et al.* and Jhou *et al.* suggested that trapped–state–assisted tunneling is a possible conduction mechanism for enhancing the dark current [5], [6]. Brazel *et al.* and Chang *et al.* suggested that there are metastable acceptor– and donor–like states coexisting in the vicinity of the surface that are responsible for high internal gains [3], [30]. The internal gain and dark current of PD_B are thus higher than those of PD_A. The inserted figure of Fig. 4(b) shows an enlarged region of the PL spectra. The intense near–band–gap transitions of samples PD_A and PD_B are located at 3.4239 and 3.4335 eV, respectively. That for the unstrained GaN layer is located at 3.4285 eV [24]. According to previous reports, the peak shift is related to the biaxial stress on the film surface [7], [24]:

$$E_g = 3.4285 \pm 0.0211\sigma_{XX}(eV) \tag{3}$$

where E_g is the intense near–band–gap transition. The biaxial stresses of samples PD_A and PD_B were calculated to be about 0.22 GPa (tensile stress) and 0.24 GPa (compressive stress), respectively. It is known that the near–band–gap transition of a semiconductor is affected by the residual stress in the film. A tensile (compressive) stress results in a decrease (increase) in the near–band–gap transition [24], [31]. In addition, the residual stress value of sample PD_A (sample S7) obtained from the PL spectra is similar to that obtained from the Raman spectra.

Fig. 5(a) and (b) show spectral responses measured from PD_A and PD_B under illumination by a xenon arc lamp, respectively. It can be seen that the cutoff is at around 360 nm for both PDs. With a 5–V applied bias, the UV–to–visible rejection ratio is defined as the responsivity measured at 360 nm divided by that measured at 420 nm. The UV–to–visible rejection ratios were estimated to be 1479 and 683 for PD_A and PD_B, respectively. Jhou *et al.* reported a UV–to–visible rejection ratio of GaN Schottky diode PDs on a sapphire substrate of about 1070, which is lower than that of PD_A [6]. With an incident light wavelength of 360 nm and a 1–V applied bias, the maximum responsivities are 0.20 and 0.25 A/W for PD_A and PD_B, respectively. The maximum responsivity of PD_A increased by 40% to 0.28 A/W when the applied bias was increased to 9–V. For PD_B, the maximum responsivity increased by 144% to 0.61 A/W when the applied bias was increased to 9–V. The significant bias–dependent responsivity of PD_B suggests that this MSM PD has a large internal gain [3], [27]. According to the previous reports, the quantum efficiency can be estimated using [3], [7], [32], [33]:

$$\eta = R \times \frac{hc}{q\lambda} \tag{4}$$

where η is the quantum efficiency, R is the measured responsivity, h is the Planck constant, c is the speed of light, q is the electron charge, and λ is the incident light wavelength. With an incident light wavelength of 360 nm and a 9–V applied bias, the maximum quantum efficiency values of PD_A and PD_B are about 97% and 210%, respectively. Notice that the maximum quantum efficiency for PD_B is larger than its theoretical limit, i.e., a quantum efficiency beyond 100%, indicating the existence of a large photoconductive gain in PD_B [3], [27], [33]. The results indicate that the small photoconductive gain of PD_A may be contributed to

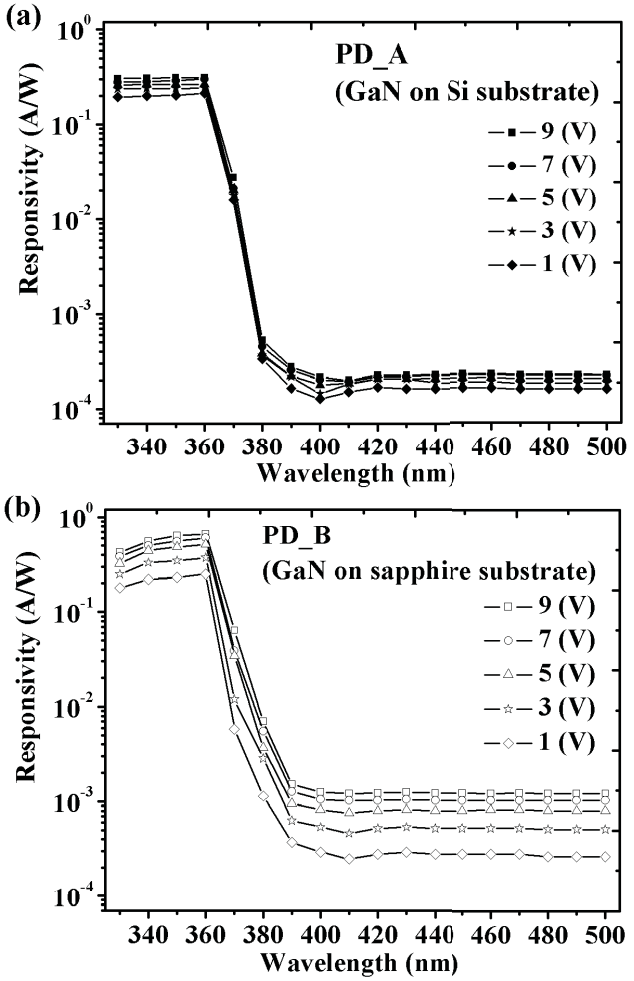

Fig. 5. Spectral responsivity of GaN MSM PDs prepared on (a) Si substrate (PD_A) and (b) sapphire substrate (PD_B).

that the high–crystal–quality epilayer on the GaN surface, which leads to a small reduction of the Schottky barrier height and a small internal gain [3], [27], [33]. With an incident light wavelength of 360 nm and a 5–V applied bias, the maximum responsivity is 0.26 A/W for PD_A, which correspond to quantum efficiencies of 90%. Chiang *et al.* reported quantum efficiencies at a 5–V applied bias for GaN MSM UV detectors prepared on an Si substrate using β–SiC (c–SiC), β–SiC (poly–SiC), and β–SiC (PSC) buffer layers of about 37%, 41%, and 47%, respectively, which are lower than those obtained here [7]. GaN–based PDs prepared on an Si substrate have better device performance, such as lower dark current and higher UV–to–visible rejection ratio, than those prepared on a conventional sapphire substrate. The results all indicate that GaN MSM PDs on an Si substrate perform well. In addition, a GaN epilayer on an Si substrate is a viable option as a template for large–area substrates and the commercial Si–based integrated circuit industry.

IV. Conclusion

A high–crystal–quality GaN epilayer was prepared on an Si substrate using VT–AlN nucleation layers and $Al_{0.3}Ga_{0.7}N$/GaN intermediate layers using metal–organic vapor–phase epitaxy. The best crystal–quality GaN epilayer was obtained with the insertion of LT–AlN nucleation layers at 993 K, 20 pairs of $Al_{0.3}Ga_{0.7}N$/GaN SL layers, and $Al_{0.3}Ga_{0.7}N$ and GaN thicknesses of 8 nm and 4 nm, respectively. The corresponding FWHM values of XRD patterns and PL spectra are about 493 arcsec and 0.032 eV, respectively. The *c*–lattice parameter of the GaN epilayer is about 5.1844 Å, which is close to that of an unstrained GaN layer (5.1850 Å). An almost–crack–free GaN surface was obtained due to tensile stress relief. With a 9–V applied bias, the dark current of UV MSM PDs on an Si substrate is about 2.4×10^{-11} A, which is one order of magnitude smaller than that of UV MSM PDs on a conventional sapphire substrate. With an incident light wavelength of 360 nm and a 9–V applied bias, the maximum quantum efficiency values of UV MSM PDs on an Si substrate is about 97%. A high–crystal–quality GaN epilayer on an Si substrate can potentially be incorporated into large–area Si–based systems.

References

[1] D. L. Mathine, "The integration of III–V optoelectronics with silicon circuitry," *IEEE J. Sel. Topics Quantum Electron.*, vol. 3, no. 3, pp. 952–959, Jun. 1997.

[2] O. Ambacher, "Growth and applications of group III-nitrides," *J. Phys. D, Appl. Phys.*, vol. 31, no. 20, pp. 2653–2710, Oct. 1998.

[3] S. J. Chang, M. L. Lee, J. K. Sheu, W. C. Lai, Y. K. Su, C. S. Chang, *et al.*, "GaN metal–semiconductor–metal photodetectors with low-temperature-GaN cap layers and ITO metal contacts," *IEEE Electron Device Lett.*, vol. 24, no. 4, pp. 212–214, Apr. 2003.

[4] S. J. Chang, S. M. Wang, P. C. Chang, C. H. Kuo, S. J. Young, and T. P. Chen, "GaN metal–semiconductor–metal photodetectors prepared on nanorod template," *IEEE Photon. Technol. Lett.*, vol. 22, no. 9, pp. 625–627, May 1, 2010.

[5] J. K. Sheu, M. L. Lee, and W. C. Lai, "Effect of low-temperature-grown GaN cap layer on reduced leakage current of GsN Schottky diodes," *Appl. Phys. Lett.*, vol. 86, no. 5, pp. 052103-1–052103-3, Jan. 2005.

[6] Y. D. Jhou, S. J. Chang, Y. K. Su, Y. Y. Lee, C. H. Liu, and H. C. Lee, "GaN Schottky barrier photodetectors with SiN/GaN nucleation layer," *Appl. Phys. Lett.*, vol. 91, no. 10, pp. 103506-1–103506-3, Sep. 2007.

[7] Y. T. Chiang, Y. K. Fang, T. H. Chou, F. R. Juang, K. C. Hsu, T. C. Wei, *et al.*, "GaN on silicon substrate with various SiC buffer layer for UV detecting applications," *IEEE Sensors J.*, vol. 10, no. 8, pp. 1291–1296, Aug. 2010.

[8] H. Yonezu, "Control of structural defects in group III–V–N alloys grown on Si," *Semicond. Sci. Technol.*, vol. 17, no. 8, pp. 762–768, Jul. 2002.

[9] S. C. Lee, B. Pattada, S. D. Hersee, Y. B. Jiang, and S. R. J. Brueck, "Nanoscale spatial phase modulation of GaN on a V-grooved Si substrate-cubic phase GaN on Si(001) for monolithic integration," *IEEE J. Quantum Electron.*, vol. 41, no. 4, pp. 596–605, Apr. 2005.

[10] H. Amano, N. Sawaki, I. Akasaki, and Y. Toyoda, "Metalorganic vapor phase epitaxial growth of a high quality GaN film using an AlN buffer layer," *Appl. Phys. Lett.*, vol. 48, no. 5, pp. 353–355, Jan. 1986.

[11] C. C. Huang, S. J. Chang, R. W. Chuang, J. C. Lin, Y. C. Cheng, and W. J. Lin, "GaN grown on Si(111) with step-graded AlGaN intermediate layers," *Appl. Surf. Sci.*, vol. 256, no. 21, pp. 6367–6370, Aug. 2010.

[12] S. F. Fang, K. Adomi, S. Iyer, H. Morkoç, H. Zabel, C. Choi, *et al.*, "Gallium arsenide and other compound semiconductors on silicon," *J. Appl. Phys.*, vol. 68, no. 7, pp. R31–R58, Oct. 1990.

[13] S. Kim, J. Oh, J. Kang, D. Kim, J. Won, J. W. Kim, *et al.*, "Two-step growth of high quality GaN using V/III ratio variation in the initial growth stage," *J. Crystal Growth*, vol. 262, no. 1–4, pp. 7–13, Feb. 2004.

[14] H. Jürgensen, "Large-scale MOVPE production systems," *Microelectron. Eng.*, vol. 18, nos. 1–2, pp. 119–148, May 1992.

[15] S. C. Jain, M. Willander, and H. Maes, "Stresses and strains in epilayers, stripes and quantum structures of III–V compound semiconductors," *Semicond. Sci. Technol.*, vol. 11, no. 5, pp. 641–671, May 1996.

[16] A. Dadgar, P. Veit, F. Schulze, J. Bläsing, A. Krtschil, H. Witte, *et al.*, "MOVPE growth of GaN on Si–substrates and strain," *Thin Solid Films*, vol. 515, no. 10, pp. 4356–4361, Mar. 2007.

[17] T. Liang, J. Tang, J. Xiong, Y. Wang, C. Xue, X. Yang, *et al.*, "Synthesis and characterization of heteroepitaxial GaN films on Si(111)," *Vacuum*, vol. 84, no. 9, pp. 1154–1158, Apr. 2010.
[18] N. A. El-Masry, J. C. Tarn, and N. H. Karam, "Interactions of dislocations in GaAs grown on Si substrates with InGaAs-GaAsP strained layered superlattices," *J. Appl. Phys.*, vol. 64, no. 7, pp. 3672–3677, Oct. 1988.
[19] R. Fischer, D. Neuman, H. Zabel, H. Morkoç, C. Choi, and N. Otsuka, "Dislocation reduction in epitaxial GaAs on Si(100)," *Appl. Phys. Lett.*, vol. 48, no. 18, pp. 1223–1225, May 1986.
[20] Y. Takano, M. Hisaka, N. Fujii, K. Suzuki, K. Kuwahara, and S. Fuke, "Reduction of threading dislocations by InGaAs interlayer in GaAs layers grown on Si substrates," *Appl. Phys. Lett.*, vol. 73, no. 20, pp. 2917–2919, Nov. 1998.
[21] A. D. Bykhovski, B. L. Gelmont, and M. S. Shur, "Elastic strain relaxation and piezoeffect in GaN-AlN, GaN-AlGaN and GaN-InGaN superlattices," *J. Appl. Phys.*, vol. 81, no. 9, pp. 6332–6338, May 1997.
[22] J. W. Yu, H. C. Lin, Z. C. Feng, L. S. Wang, S. Tripathy, and S. J. Chua, "Control and improvement of crystalline cracking from GaN thin films grown on Si by metalorganic chemical vapor deposition," *Thin Solid Films*, vol. 498, nos. 1–2, pp. 108–112, Mar. 2006.
[23] S. Tripathy, S. J. Chua, P. Chen, and Z. L. Miao, "Micro-Raman investigation of strain in GaN and $Al_xGa_{1-x}N$/GaN heterostructures grown on Si(111)," *J. Appl. Phys.*, vol. 92, no. 7, pp. 3503–3510, Oct. 2002.
[24] D. G. Zhao, S. J. Xu, M. H. Xie, S. Y. Tong, and H. Yang, "Stress and its effect on optical properties of GaN epilayers grown on Si(111), 6H–SiC, and c-plane sapphire," *Appl. Phys. Lett.*, vol. 83, no. 4, pp. 677–679, Jul. 2003.
[25] V. S. Harutyunyan, A. P. Aivazyan, E. R. Weber, Y. Kim, Y. Park, and S. G. Subramanya, "High-resolution X-ray diffraction strain-stress analysis of GaN/sapphire heteropstrucures," *J. Phys. D, Appl. Phys.*, vol. 34, no. 10A, pp. A35–A39, May 2001.
[26] M. K. Öztürk, H. Altuntaş, S. Çörekçi, Y. Hongbo, S. Özçelik, and E. Özbay, "Strain–stress analysis of AlGaN/GaN heterostructures with and without an AlN buffer and interlayer," *Strain*, vol. 47, pp. 19–27, Jun. 2010.
[27] O. Katz, V. Garber, B. Meyler, G. Bahir, and J. Salzman, "Gain mechanism in GaN Schottky ultraviolet detectors," *Appl. Phys. Lett.*, vol. 79, no. 10, pp. 1417–1419, Sep. 2001.
[28] W. Grieshaber, E. F. Schubert, I. D. Goepfert, R. F. Karlicek, M. J. Schurman, and C. Tran, "Competition between band gap and yellow luminescence in GaN and its relevance for optoelectronic devices," *J. Appl. Phys.*, vol. 80, no. 8, pp. 4615–4620, Oct. 1996.
[29] S. J. Chung, O. H. Cha, C. H. Hong, E. K. Suh, H. J. Lee, Y. S. Kim, *et al.*, "Emission mechanism of the yellow luminescence in undoped GaN," *J. Korean Phys. Soc.*, vol. 37, no. 6, pp. 1003–1006, Dec. 2000.
[30] E. G. Brazel, M. A. Chin, and V. Narayanamurti, "Direct observation of localized high current densities in GaN films," *Appl. Phys. Lett.*, vol. 74, no. 16, pp. 2367–2369, Apr. 1999.
[31] Y.-Y. Fang, J. Tolle, J. Tice, A. V. G. Chizmeshya, J. Kouvetakis, V. R. D'Costa, *et al.*, "Epitaxy-driven synthesis of elemental Ge/Si strain-engineered materials and device structures via designer molecular chemistry," *Chem. Mater.*, vol. 19, no. 24, pp. 5910–5925, Oct. 2007.
[32] C. K. Wang, S. J. Chang, Y. K. Su, Y. Z. Chiou, S. C. Chen, C. S. Chang, *et al.*, "GaN MSM UV photodetectors with titanium tungsten transparent electrodes," *IEEE Trans. Electron Devices*, vol. 53, no. 1, pp. 38–42, Jan. 2006.
[33] S. J. Chang, C. L. Yu, R. W. Chung, P. C. Chang, Y. C. Lin, Y. W. Jhan, *et al.*, "Nitride-based MIS-like photodiodes with semiinsulating Mg-doped GaN cap layers," *IEEE Sensors J.*, vol. 6, no. 5, pp. 1043–1044, Oct. 2006.

Chao-Wei Hsu received the Ph.D. and M.S. degrees from the Institute of Microelectronics and the Institute of Nanotechnology and Microsystems Engineering, National Cheng Kung University, Tainan, Taiwan.

He has worked for Taiwan Semiconductor Manufacturing Company Limited, Industrial Technology Research Institute, and Chang Gung Memorial Hospital, Taiwan. His research interests include III–V compound devices, microelectronics, microsystems, nanotechnology, and biotechnology.

Yung-Feng Chen received the Ph.D. and B.S. degrees in materials science and engineering from National Cheng Kung University, Tainan, Taiwan.

He currently works in the Department of Electrical Engineering, Advanced Optoelectronic Technology Center, National Cheng Kung University. His main research interests include kaolin–Al_2O_3 ceramics, III–V compound materials and devices, device process integration, and advanced materials research and analysis.

Yan-Kuin Su (F'06) received the Ph.D. and B.S. degrees in electrical engineering from National Cheng Kung University (NCKU), Tainan, Taiwan. From 1979 to 1983, he was with the Department of Electrical Engineering, NCKU, as an Associate Professor and was engaged in research on compound semiconductors and optoelectronic materials. In 1983, he was promoted to Full Professor.

From 1979 to 1980 and 1986 to 1987, he was on leave, working at the University of Southern California, Los Angeles, and AT&T Bell Laboratories, as a Visiting Scholar. He was also a Visiting Professor with Stuttgart University, Germany, in 1993. In 1991, he became an Adjunct Professor with the State University of New York, Binghamton. He is currently a Professor in the Department of Electrical Engineering at NCKU and the Director General of the Department of Engineering and Applied Science, National Science Council. His research activities have been in compound semiconductors, integrated optics, and microwave devices. He has published over 200 papers in the area of thin-film materials and devices and optoelectronic devices.

Prof. Su is a member of The International Society for Optical Engineers, the Materials Research Society, and Phi Tau Phi. He received the Outstanding Research Professor Fellowship from the National Science Council, from 1986 to 1992 and 1994 to 1995. He received the Best Teaching Professor Fellowship from the Ministry of Education, Taiwan, in 1992. In 1995, he received the Excellent Engineering Professor Fellowship from the Chinese Engineering Association. In 1996 and 1998, he received the Award from the Chinese Electrical Engineering Association. In 1998, he received the Academy Member of Asia-Pacific Academy of Materials.